BAMS Article

Exploring Snowfall Variability through the High-Latitude Measurement of Snowfall (HiLaMS) Field Campaign

Steven J. Cooper, Tristan S. L'Ecuyer, Mareile Astrid Wolff, Thomas Kuhn, Claire Pettersen, Norman B. Wood, Salomon Eliasson, Claire E. Schirle, Julia Shates, Franziska Hellmuth, Bjørg Jenny Kokkvoll Engdahl, Sandra Vásquez-Martín, Trond Ilmo, and Knut Nygård

ABSTRACT: The High-Latitude Measurement of Snowfall (HiLaMS) campaign explored variability in snowfall properties and processes at meteorologically distinct field sites located in Haukeliseter, Norway, and Kiruna, Sweden, during the winters of 2016/17 and 2017/18, respectively. Campaign activities were founded upon the sensitivities of a low-cost, core instrumentation suite consisting of Micro Rain Radar, Precipitation Imaging Package, and Multi-Angle Snow Camera. These instruments are highly portable to remote field sites and, considered together, provide a unique and complementary set of snowfall observations including snowflake habit, particle size distributions, fall speeds, surface snowfall accumulations, and vertical profiles of radar moments and snow water content. These snow-specific parameters, used in combination with existing observations from the field sites such as snow gauge accumulations and ambient weather conditions, allow for advanced studies of snowfall processes. HiLaMS observations were used to 1) successfully develop a combined radar and in situ microphysical property retrieval scheme to estimate both surface snowfall accumulation and the vertical profile of snow water content, 2) identify the predominant snowfall regimes at Haukeliseter and Kiruna and characterize associated macrophysical and microphysical properties, snowfall production, and meteorological conditions, and 3) identify biases in the HARMONIE-AROME numerical weather prediction model for forecasts of snowfall accumulations and vertical profiles of snow water content for the distinct snowfall regimes observed at the mountainous Haukeliseter site. HiLaMS activities and results suggest value in the deployment of this enhanced snow observing instrumentation suite to new and diverse high-latitude locations that may be underrepresented in climate and weather process studies.

KEYWORDS: Climate variability; Ice crystals; Snow cover; In situ atmospheric observations; Radars/Radar observations; Numerical weather prediction/forecasting

https://doi.org/10.1175/BAMS-D-21-0007.1

Corresponding author: Steven J. Cooper, steve.cooper@utah.edu

In final form 26 April 2022

AFFILIATIONS: Cooper and Schirle—Department of Atmospheric Sciences, University of Utah, Salt Lake City, Utah; **L'Ecuyer and Shates**—Department of Atmospheric and Oceanic Sciences, University of Wisconsin–Madison, Madison, Wisconsin; **Wolff, Engdahl, Ilmo, and Nygård**—Norwegian Meteorological Institute, Oslo, Norway; **Kuhn and Vásquez-Martín**—Luleå University of Technology, Kiruna, Sweden; **Pettersen**—Space Science and Engineering Center, University of Wisconsin–Madison, Madison, Wisconsin, and Climate and Space Sciences and Engineering, University of Michigan, Ann Arbor, Michigan; **Wood**—Space Science and Engineering Center, University of Wisconsin–Madison, Madison, Wisconsin; **Eliasson**—Swedish Meteorological and Hydrological Institute, Norrköping, Sweden; **Hellmuth**—University of Oslo, Oslo, Norway

The High-Latitude Measurement of Snowfall (HiLaMS) field campaign sought an improved understanding of snowfall properties and processes at two meteorologically distinct field sites in Scandinavia during the winters of 2016/17 and 2017/18. HiLaMS science featured a synergistic in situ measurement–remote sensing–numerical modeling design using techniques developed by project partners from the University of Utah and University of Wisconsin in the United States and the Norwegian Meteorological Institute (MET-Norway), the University of Oslo (UiO), Swedish Meteorological and Hydrological Institute (SMHI), and Luleå University of Technology (LTU) in Scandinavia. The winter 2016/17 deployment was at the MET-Norway Haukeliseter test site in the mountainous Telemark region of Norway, while the winter 2017/18 campaign was at a generally colder and drier Arctic observation site near Kiruna at the Swedish Institute of Space Physics (IRF) run by LTU. Figures 1 and 2 show site images and topographical maps, respectively. Core project instrumentation included the Micro Rain Radar (MRR; Klugmann et al. 1996), Precipitation Imaging Package (PIP; Pettersen et al. 2020a, 2021), and Multi-Angle Snow Camera (MASC; Garrett et al. 2012). These instruments generate a unique and complementary set of snowfall observations including snow particle size distributions (PSD), habit, and fall speeds, and vertical profiles of radar reflectivity from which profiles of snow water content (SWC) can be derived. These parameters provide the basis for mapping regional snowfall characteristics, evaluating forecasts and model physics, and supporting advanced studies of snowfall processes and impacts when used in combination with coincident atmospheric-state and snowfall observations from Scandinavian-partner field sites.

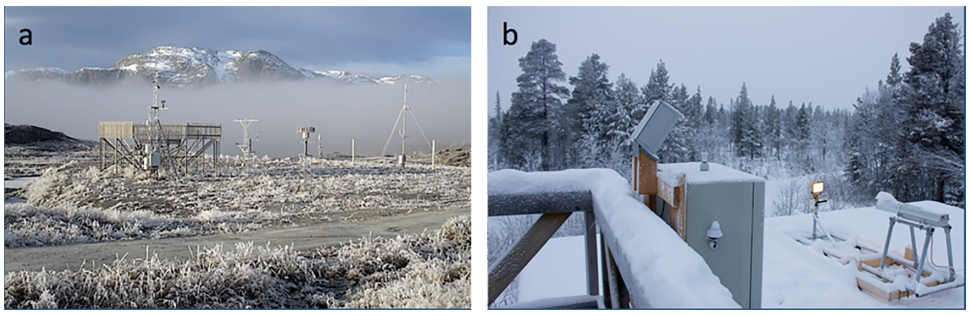

Fig. 1. (a) The MET-Norway Haukeliseter test site, which sits above tree line in the mountains of Telemark. (b) The IRF site in Kiruna, which is located in a boreal forest above the Arctic Circle in northern Sweden.

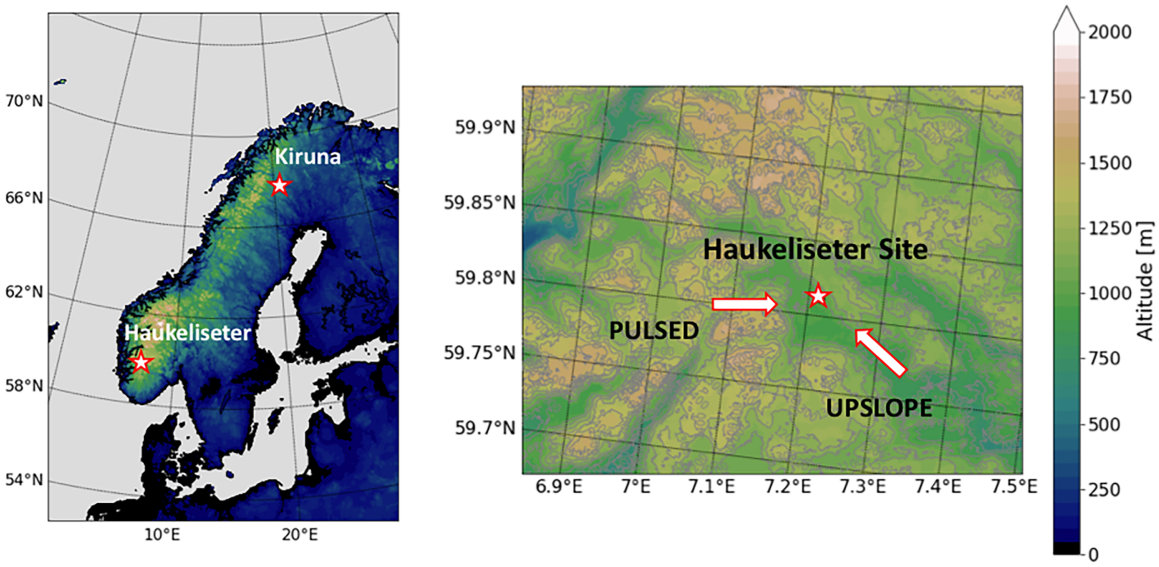

Fig. 2. (a) Location of HiLaMS field sites at Haukeliseter, Norway, in winter 2016/17 and Kiruna, Sweden, in winter 2017/18. (b) Topography and surface wind direction for two snowfall regimes observed at the Haukeliseter test site. Figure from S19.

The high-latitude regions are undergoing some of the largest transformations attributed to climate change, exemplified through a collection of processes referred to as Arctic amplification (Manabe and Stouffer 1980; Chapman and Walsh 1993; Nicholls et al. 1996; Holland and Bitz 2003; Serreze and Francis 2006; Bekryaev et al. 2010; Crook et al. 2011; Serreze and Barry 2011). The fundamental role of snowfall in these scenarios is understood well to the first order. Changes in the spatial distribution of snowfall and ice cover in high-latitude regions in response to anthropogenic warming feedback on the climate system through impacts on albedo and surface energy budgets (Cohen and Rind 1991; Brown 2000; Holland et al. 2006; Vavrus 2007; Screen and Simmonds 2010; Cohen et al. 2012; Bindoff et al. 2013). Snowfall accumulation also acts to build and maintain the Antarctic and Greenland ice sheets and, therefore, is an important variable when considering projections of sea level rise (Shepherd and Wingham 2007; Jacob et al. 2012; Gardner et al. 2013; Lenaerts et al. 2013; Palerme et al. 2014, 2017).

Snowfall at weather time scales has wide-ranging societal impacts. Although surface snowfall may be viewed most simply as an end product of the snow event, the snowfall itself also interacts with and influences the overall storm environment and exerts lasting influences on the energy and water cycles. The effects of snowfall on its immediate environment are easily recognized in that it transports water mass to the surface and thus can modify surface albedo, emissivity, and other properties relevant to energy balance that may impact cloud growth and lifetime. For example, snow cover has been shown to act as a fast climate switch influencing air temperature, cloud cover, and boundary layer structure (Betts et al. 2014). Vertical profiles of snow microphysical properties also help dictate snow event evolution as diabatic heating generated from snow formation processes modulates potential vorticity in synoptic-scale disturbances (Joos and Wernli 2012; Schäfler et al. 2018).

Considerable progress has been made on understanding the physics behind the atmosphere–surface interactions that drive these climate and weather feedback processes (e.g., Curry et al. 1996; Shupe and Intreiri 2004; Morrison et al. 2012; Bennartz et al. 2013; Van Tricht et al. 2016; McIlhattan et al. 2017; Pettersen et al. 2018). Much of this work was facilitated through use of measurements from high-latitude supersite observatories, specifically the Atmospheric Radiation Measurement (ARM) North Slope of Alaska (NSA) Climate Facility at Barrow (now Utqiaġvik) and the Integrated Characterization of Energy, Clouds, Atmospheric

state, and Precipitation at Summit (ICECAPS; Shupe et al. 2013) project on Greenland. Numerous high-latitude field campaigns also were implemented to characterize high-latitude snowfall processes (Intrieri et al. 2002; Verlinde et al. 2007; Tjernström et al. 2014; Smith et al. 2017; Wendisch et al. 2019). Recent campaigns included the Multidisciplinary drifting Observatory for the Study of Arctic Climate (MOSAiC; Shupe et al. 2022) and ARM Cold-Air Outbreaks in the Marine Boundary Layer Experiment (COMBLE; Geerts 2019) field programs that sought to reduce documented gaps in our understanding of cloud, precipitation, and surface processes and their relationships with boundary layer and synoptic-scale controls.

Despite these efforts, key uncertainties remain in our understanding of the overall impact of snowfall on climate and weather. These gaps are due, in part, to limitations in existing snow observations in the remote high-latitude regions and oftentimes large uncertainties in satellite-derived snowfall products (e.g., Kulie and Bennartz 2009). These concerns were highlighted in the National Science Foundation (NSF) "10 Big Ideas for Future NSF Investments" program that stressed that "current Arctic observations are sparse and inadequate for enabling discovery or simulation of the processes underlying Arctic system." In the spirit of these concerns, the HiLaMS campaign was conceived to attack key remaining research questions in our understanding of high-latitude snowfall. For example, we have not yet quantified the amount of snow generated under varying high-latitude storm systems and have not adequately assessed the resulting impact of this snow on the variables like surface albedo that drive the surface energy and mass balance. These are, however, primary pathways by which systematic shifts in high-latitude weather states may feedback on climate. Lacking observational constraints for the diverse climate regimes found across the high latitudes, model representations of key feedback processes underlying Arctic amplification may be incomplete or biased to an unknown degree.

During HiLaMS, simultaneous MRR, PIP, and MASC observations were made to generate complementary estimates of snowfall properties including snow particle habit, PSD, particle fall speeds, surface snowfall accumulations, and SWC. This core instrumentation package is highly portable and requires much less power relative to larger facilities, allowing for ease in deployment to remote field locations that may lack extensive infrastructure or logistical support. This flexibility permits the generation of unique low-cost datasets for locations and climates that may be underrepresented in process studies. During HiLaMS, for example, we pursued snowfall process studies for an Alpine tundra environment in Norway and an Arctic boreal forest location in Sweden. As such, the meteorological conditions observed during HiLaMS contrast starkly with those at the ARM or ICECAPS supersites in the high Arctic or those during the much larger MOSAiC and COMBLE field campaigns that focused on maritime environments. Such efforts complement existing longer-term snowfall observation sites in unique high-latitude locations including Hyytiälä station in Finland (Petäjä et al. 2016) and the Dumont d'Urville Station in Antarctica (Berne et al. 2017; Grazioli et al. 2017).

This paper describes the MRR–PIP–MASC instrumentation suite and its deployment to the Haukeliseter test site in winter 2016/17 and to the Kiruna IRF site in winter 2017/18. We discuss previously peer-reviewed results from the application of data collected during these Swedish and Norwegian deployments to 1) develop a variational, combined radar and in situ microphysical property retrieval scheme to estimate both surface snowfall accumulations and the vertical profile of SWC (Schirle et al. 2019, hereafter S19), 2) identify the predominant snowfall regimes at Haukeliseter and Kiruna and characterize their macrophysical and microphysical properties, snowfall production, and meteorological conditions (Shates et al. 2021), and 3) quantify the ability of the HARMONIE-AROME numerical weather prediction (NWP) model (Seity et al. 2011; Brousseau et al. 2016; Bengtsson et al. 2017) to predict surface snowfall accumulations and profiles of SWC for the snowfall regimes observed at the mountainous Haukeliseter site (Hellmuth et al. 2021). Finally, we explore possible experimental

designs linking the hydrological, dynamical, and radiative processes of snowfall that flow directly from the MRR–PIP–MASC observations presented here when augmented by additional instrumentation or analyses techniques from the broader atmospheric community.

Instrumentation and research sites

HiLaMS science objectives were founded upon the complementary sensitivities of the core MRR–PIP–MASC instrumentation suite. Figure 3a shows the arrangement of these sensors at the Haukeliseter test site. We note that the MASC became inoperative during year 1 at Haukeliseter during extreme weather event Urd but not before it had photographed hundreds of thousands of hydrometeors. During the year 2 deployment at Kiruna, a Dual Ice Crystal Imager (D-ICI; Kuhn and Vázquez-Martín 2020) developed at LTU provided information on particle snowflake habit in lieu of MASC observations.

MRR. The METEK MRR 2 is a frequency-modulated, continuous-wave, vertically pointing radar that operates at a frequency of 24 GHz (Klugmann et al. 1996). It provides observations of effective reflectivity, Doppler velocity, and spectral width. A noise removal technique is applied to the MRR observations to increase radar sensitivity to an effective reflectivity of −10 dBZe (Maahn and Kollias 2012) and limit effects of interference (Pettersen et al. 2020b). Reflectivity observations provide a description of storm macrophysical structure and are used to derive SWC aloft. MRR Doppler velocity observations are used to estimate particle fall speeds, which are required to translate SWC into snowfall rate. Figure 4 shows typical MRR reflectivity and Doppler velocity profiles and values for two snowfall regimes observed at Haukeliseter during HiLaMS. As with all radars, careful calibration of the MRR over time is critical for the generation of accurate long-term observations of reflectivity (Kollias et al. 2019; Myagkov et al. 2020).

PIP. The PIP video imager captures images of falling hydrometeors from which snow PSDs and fall speeds can be derived (Pettersen et al. 2020a, 2021), both for use as inputs in the radar-based snowfall retrieval algorithm and in regime-dependent microphysical analyses. The PIP consists of a high-speed video camera located ~2 m away from a halogen lamp which illuminates falling precipitation. This design reduces the creation of turbulence from the apparatus itself and samples a very large volume relative to other optical probes, thus providing measurements of PSD and particle motions that likely are an accurate representation of the snow conditions during an event. The bottom panel in Fig. 5a shows PSDs derived from PIP observations for a sample snow event at Haukeliseter.

MASC. The MASC captures high-resolution images of falling snow from which estimates of particle shape, maximum dimension, and fall speed can be found for each falling snowflake

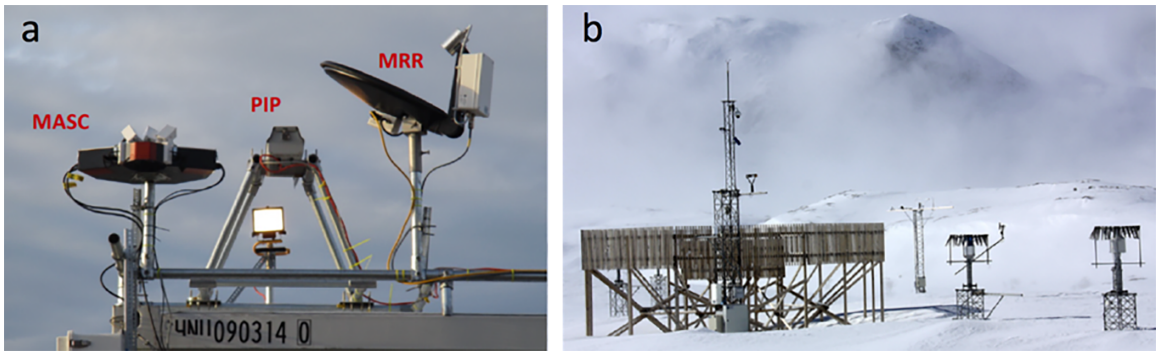

Fig. 3. (a) The experimental setup for the deployment of the MRR, MASC, and PIP at the MET-Norway Haukeliseter test site during HiLaMS in 2016/17. (b) MET-Norway DFAR and single fence snow gauges at the site. Figure modified from S19.

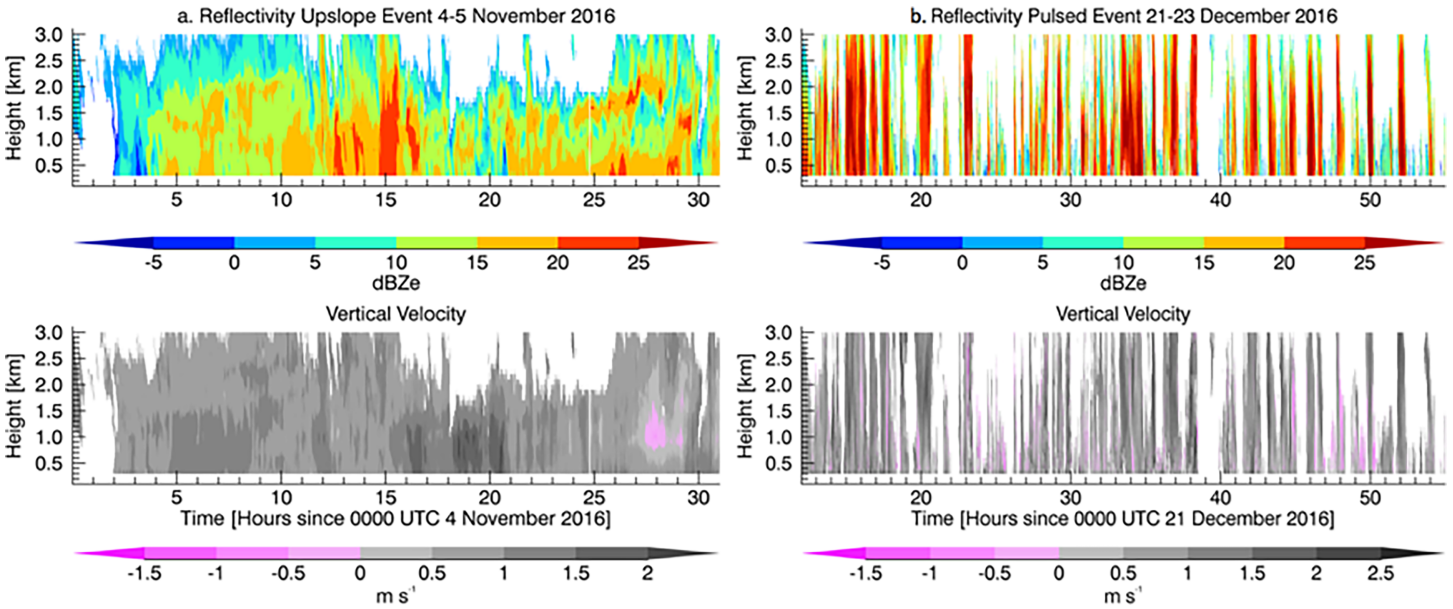

Fig. 4. (a) Typical MRR reflectivity and Doppler velocity signatures associated with the "upslope" snowfall regime seen at Haukeliseter. (b) As in (a), but for a "pulsed" snowfall event. Negative velocities denote upward motion. Figure modified from S19.

(Garrett et al. 2012). Particle shape observations are critical for the radar-based snowfall retrieval algorithm as they provide guidance for the selection of an appropriate particle model for a given snowfall scene. In design, the MASC employs three cameras pointed toward a common focal point in the center of the instrument sampling ring. As snowflakes fall through this sampling ring, they activate two near-infrared sensors that trigger the cameras. The MASC determines the fall speed of the snowflake by measuring the time it takes to fall between the vertically aligned infrared sensors. Figure 5b shows sample MASC images from Haukeliseter. The top panel in Fig. 5a shows sample PSD estimates derived from MASC images. Side-by-side comparisons of PSD estimates from the MASC and PIP as in Fig. 5a suggested possible MASC sampling biases as discussed in S19. Therefore, HiLaMS science applications were based upon the understanding that the MASC provided useful information on particle habit whereas the PIP provided a more complete description of PSD.

MET-Norway Haukeliseter test site. The Norwegian component of the HiLaMS campaign took place from October 2016 to April 2017 at the Haukeliseter test site in the mountainous Telemark region of central Norway; see Figs. 1–3. This Alpine site is located above tree line at an elevation of 991 m at 59.8°N on the southern edge of the Hardangervidda mountain plateau. Haukeliseter was ideal for HiLaMS given its persistent snowfall and seven month long winters (Wolff et al. 2015). Proximity to the moist Gulf Stream provided the opportunity to observe snowstorms that generate heavy riming (S19), such as intense atmospheric river events (illustrated in Fig. 4b) that can have severe impacts on northern European communities (Stohl et al. 2008).

MET-Norway has equipped the Haukeliseter test site with multiple precipitation gauges, thermometers, anemometers, and other basic meteorological observations necessary for HiLaMS snowfall analyses. Geonor T-200B3 precipitation gauges located either inside a double fence intercomparison reference (DFIR; Goodison et al. 1998), denoted as a double fence automated reference (DFAR; Kochendorfer et al. 2018), or inside a single Alter wind shield provide measurements of liquid water equivalent of snow accumulation at 1-min temporal resolution. DFAR and single fence gauges are shown in Fig. 3b. The DFAR provides more

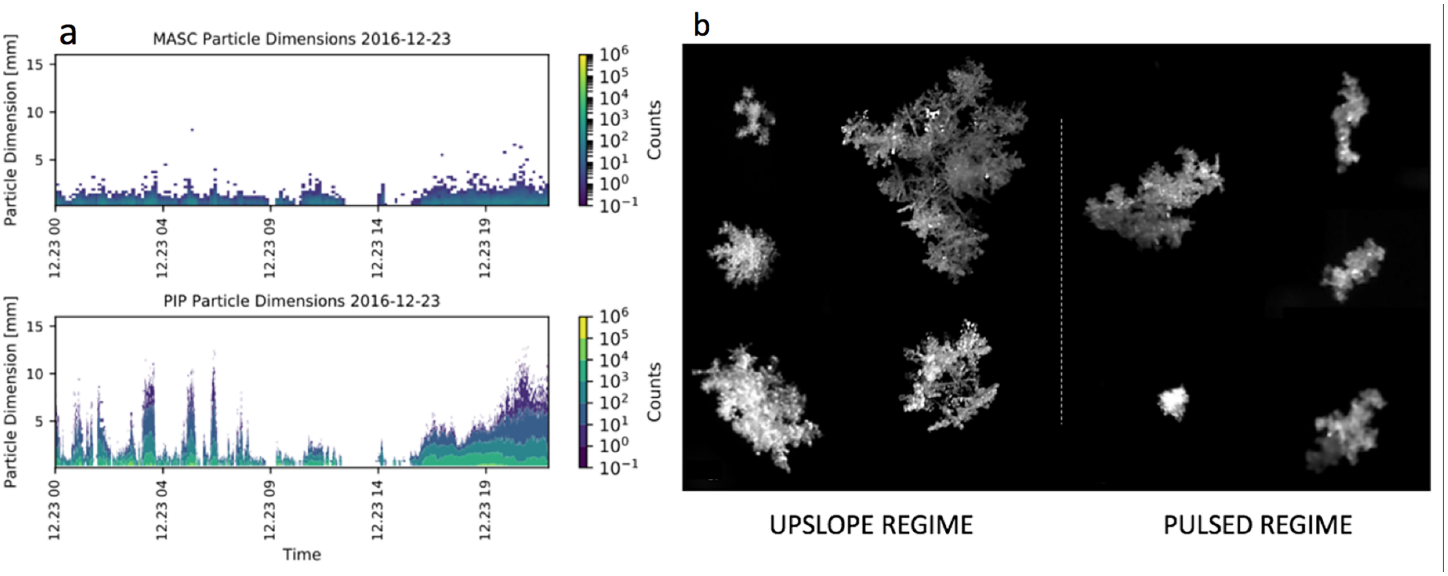

Fig. 5. (a) MASC and PIP observed particle size distributions for a 23 Dec snow event at Haukeliseter. (b) Typical rimed snow particles observed at the site for both upslope and pulsed storm regimes. Figure modified from S19.

accurate estimates of snowfall accumulations than the single fence gauges, especially in windy conditions such as those found at Haukeliseter (Rasmussen et al. 2012; Wolff et al. 2015; Kochendorfer et al. 2018, 2022). The DFAR therefore is considered as "best truth" for these studies. Mast-mounted anemometers at a height of 10 m provided wind direction and speed measurements. The "Haukeliseter snow gauge studies" sidebar describes the snowfall-related work pursued by MET-Norway at the site in more detail.

Haukeliseter snow gauge studies

The Norwegian Meteorological Institute established the Haukeliseter test site for the study of precipitation processes in the mountainous Telemark region of central Norway in 2011. The site (Fig. SB1) is located well above tree line near an altitude of 1,000 m on a relative plateau with surrounding mountaintops of 1,200–1,500 m located 1–4 km away. Natural vegetation is dominated by low scrubs and moss. The winter season lasts from October to May and exhibits precipitation events primarily in the form of snow and sleet that can have sustained windspeeds up to 20 m s^{-1} and temperatures as low as –30°C. These conditions, together with the relative homogeneity of the location (Wolff et al. 2013), make the site ideal to study measurement performances of different precipitation sensors and configurations under extreme winter conditions.

Fig. SB1. The MET-Norway Haukeliseter test site provides researchers with year-round access to advanced instrumentation in a remote Alpine, tundra setting.

At the heart of Haukeliseter science lies a DFAR, a field working reference system defined by the World Meteorological Organization (WMO) for the measurement of solid precipitation. The accurate measurement of snowfall amount from precipitation gauges is notoriously challenging (Goodison et al. 1998; Rasmussen et al. 2012). During windy conditions, falling snowflakes may be unable to settle in the snow gauge opening, resulting in the underestimation of snowfall amount. With the DFAR, however, the outer fence reduces wind speed and turbulence for the falling snowflakes within the inner fence, improving the likelihood that they settle into the precipitation gauge and providing more accurate estimates of snowfall.

Wolff et al. (2015) used DFAR observations at Haukeliseter to develop an adjustment function for the wind induced undercatch in solid and mixed precipitation measurements by the Geonor gauge with Alter wind shield, the standard configuration of single fence precipitation gauges in the Norwegian network. Use of coincident optical precipitation sensors and basic meteorological observations allowed for scene-dependent analyses of snow gauge performance as a function of wind speed, temperature, or other environmental variables. Overall, the single fence gauges showed an undercatch of approximately 50% of total precipitation over monthly and seasonal time scales during typical winters. Use of the adjustment function reduced the bias in estimated precipitation to about 10%.

The MET-Norway site also was included in the WMO Solid Intercomparison Experiment (WMO-SPICE; Nitu et al. 2018). In that program, Kochendorfer et al. (2017) developed a universal adjustment function based on the data from Haukeliseter and various WMO-SPICE sites that was further evaluated by Kochendorfer et al. (2018) and Smith et al. (2020). Although this universal approach again succeeded in reducing measurement bias from precipitation observations on a seasonal basis, its use could suggest significantly too little or too much snowfall for individual snow events and specific sites. Such findings dictate the need for the continued study of the impact of local topography, meteorological conditions, and snow particle microphysical properties on snow gauge sampling efficiencies (Kochendorfer et al. 2021).

Kiruna IRF site. The Swedish component of the HiLaMS field campaign took place from September 2017 to May 2018 at the IRF site operated by LTU near Kiruna at 67.8°N; see Figs. 1 and 2. The site was selected as it experiences frequent and measurable snowfall from September through May and its taiga climate contrasts significantly with that of Haukeliseter. It is located at an elevation of 425 m in a region surrounded by forests with proglacial lakes and discontinuous permafrost (Gisnås et al. 2017). Sweden's highest mountains are approximately 75 km southwest of Kiruna and limit the influence of the relatively warm Atlantic Ocean on this inland site.

The IRF location provided multiple field site options for HiLaMS instrumentation and housed the basic meteorological observations necessary for project process studies. The MRR was located on the roof of the main IRF building, whereas the PIP and D-ICI were mounted approximately 0.4 km away atop the one-story IRF lidar laboratory. Existing site instrumentation included a Vaisala WXT536, which provided 1-min observations of wind speed and direction, surface temperature, and relative humidity at 2 m above ground level. Snowfall accumulation measurements were available from single-fence snow gauges at the SMHI weather station at Jukkasjärvi, which is located several kilometers to east of IRF. Given the relatively homogenous forest conditions, the small distances between project instrumentation are much less of an issue than it would be in the complex Haukeliseter topography.

Deploying at Kiruna also enabled coincident measurements with the D-ICI, a ground-based in situ instrument developed at LTU to determine snow ice crystal properties and fall speed simultaneously (Kuhn and Vázquez-Martín 2020). The instrument takes high-resolution pictures of the same falling ice particle from two different viewing directions. One viewing direction is horizontal and is used to determine fall speed by means of a double exposure. The "Kiruna D-ICI studies" sidebar describes D-ICI science applications at Kiruna in detail.

Kiruna D-ICI studies

The D-ICI is a high-resolution in situ instrument used for capturing key parameters of falling snow particles. Vertically and horizontally pointing cameras take images of single particles that pass through the inlet's sensing volume, enabling the simultaneous retrieval of snow crystal properties and fall speed (Kuhn and Vázquez-Martín 2020) for particles within the 20 μm–3.2 mm range. The vertically viewing camera captures the size and shape of the snow particles from single-exposure images. The horizontally viewing camera uses a double exposure technique to determine fall speed. This combination of geometries is ideal for linking particle shape and size to fall speed since properties seen from the vertical direction have the most significant impact on fall speed.

The use of both D-ICI view angles significantly reduces the ambiguities of particle shape classification relative to a single viewing geometry. The images of snowflakes in Fig. SB2 demonstrate this concept. In Fig. SB2a, the attached bullet is seen only from the side view. In Fig. SB2b, a plate would be mistaken for a needle given the side view alone.

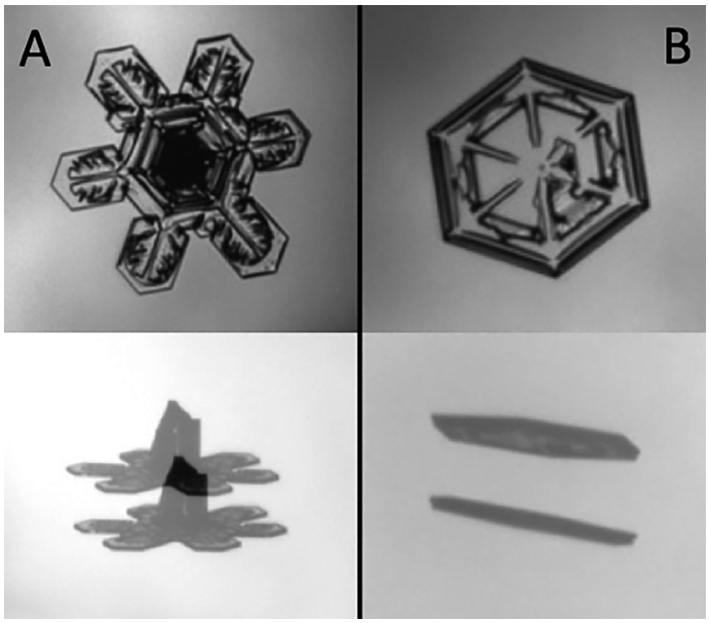

Fig. SB2. Examples of D-ICI dual images of snowflakes with (top) top view and (bottom) side view.

The deployment of D-ICI at the Kiruna site during the snowfall seasons of 2014–19 produced a dataset of snow particle properties including particle shape, size parameter, and fall speed (Vázquez-Martín et al. 2021a). Particle shape classification from this dataset led to an update of the widely used scheme by Magono and Lee (Vázquez-Martín et al. 2020). Determination of mass for simpler particle shapes from geometry considerations allowed for the verification of the size parameter best suited to determine Reynolds number and the evaluation of particle mass–fall speed relationships (Vázquez-Martín et al. 2021b). Future deployments of D-ICI are planned for applications where the shape of snow particles is important, such as in complementing cloud radar and disdrometers for EarthCARE snowfall validation activities. While D-ICI was originally developed for smaller snow crystals, future versions will include a wider field of view to identify a broader particle size range and to improve automated image processing and shape recognition.

HiLaMS science highlights

The HiLaMS campaign sought an improved understanding of snowfall properties and processes at the meteorologically distinct Haukeliseter and Kiruna sites in Scandinavia using a combination of in situ measurements, remote sensing observations, and numerical modeling techniques. This section describes key scientific achievements from HiLaMS.

Successfully creating research quality data streams from HiLaMS instrumentation required the use of advanced snowfall remote sensing techniques that translate observations

into accurate estimates of snowfall properties. For the conversion of radar reflectivities into estimates of snow water, we exploited our long heritage of snowfall-related activities centered around the *CloudSat* 94-GHz Cloud Profiling Radar (CPR) and its 2C-SNOW-PROFILE snowfall product (Wood and L'Ecuyer 2018, 2021). The CPR retrieval scheme exploits the flexible optimal-estimation approach (Rodgers 2000) to combine radar reflectivities, PSD–temperature parameterizations, and environmental profiles into a common framework to derive a best estimate of snowfall properties consistent with each. The accuracy of any snowfall retrieval scheme, however, depends upon the selection of a particle model (mass–dimension–reflectivity relationships) well matched to scene meteorological conditions (Cooper et al. 2017, S19).

For HiLaMS, we considered snow particle models (Wood et al. 2015) that were designed for the *CloudSat* algorithm based on observations from the Canadian *CloudSat–CALIPSO* Validation Project (C3VP; Hudak et al. 2006) and discrete dipole approximation simulations of scattering properties (Draine and Flatau 1994). This collection of physically based particle models allowed for the selection of an appropriate particle model for the retrieval scheme based upon observed snowflakes for a given snow event. These particle models were intended to simulate the coarse features of snow particles and consisted of solid-ice dipoles intermixed with empty dipole locations to meet observed mass and horizontally projected area constraints. For simplicity, we focus the discussion on two particles, B6pf and B8pr-30 (Wood et al. 2015), that have markedly different maximum dimension–backscatter relationships. The B6pf will hereafter be referred to as the "reflective aggregate" (RA) particle as it produced high reflectivities per unit mass relative to the B8pr-30, hereafter designated as the "less reflective aggregate" (LRA) particle. Use of the *CloudSat* particle models for the Scandinavian sites had the additional benefit of identifying potential scene-dependent biases in the 2C-SNOW PROFILE product.

Combined radar, in situ snowfall retrieval scheme. The core MRR–PIP–MASC instrumentation suite provided an ideal opportunity to explore our ability to characterize the vertical profile of snow properties as a function of snowfall regime. Such efforts are critical as accurate descriptions of these properties provide the scientific foundation for snowfall process studies. Radar reflectivities are commonly used to estimate SWC aloft or surface snowfall rates, although this translation from reflectivity space to physical space is challenging and nonunique (Kulie and Bennartz 2009; Cooper et al. 2017). Essentially, the use of different but reasonable assumptions of snowfall microphysical properties, such as particle model or PSD, in the inversion can lead to large differences in estimated snow water for given radar reflectivities.

S19 modified a combined radar and in situ snowflake microphysical property retrieval scheme originally developed for instrumentation at ARM Barrow (Cooper et al. 2017) to HiLaMS instrumentation. Specifically, PSD observations derived from the PIP and a particle model consistent with MASC images of snowflakes were used as input in an MRR reflectivity retrieval scheme. At the Haukeliseter test site, MASC images suggested primarily rimed aggregates across snow events as shown in Fig. 5b. As such, we selected the compact RA particle model for the retrieval scheme that could produce the large backscatters expected from snow particles entrained in a high liquid water content environment aloft. Fall speed estimates necessary to convert SWC to snowfall rate were available from each the PIP, MASC, and MRR. Retrieved surface snowfall accumulations were evaluated against MET-Norway DFAR observations to quantify retrieval performance for the snowfall regimes observed at Haukeliseter.

Analyses of MRR reflectivities and basic meteorological observations suggested two predominant snowfall regimes at the Haukeliseter test site during HiLaMS. One snowfall regime exhibited continuous but moderate snowfall and formed with light winds from the southeast. From the topographical map in Fig. 2b, these winds suggest gently lifting "upslope" motion

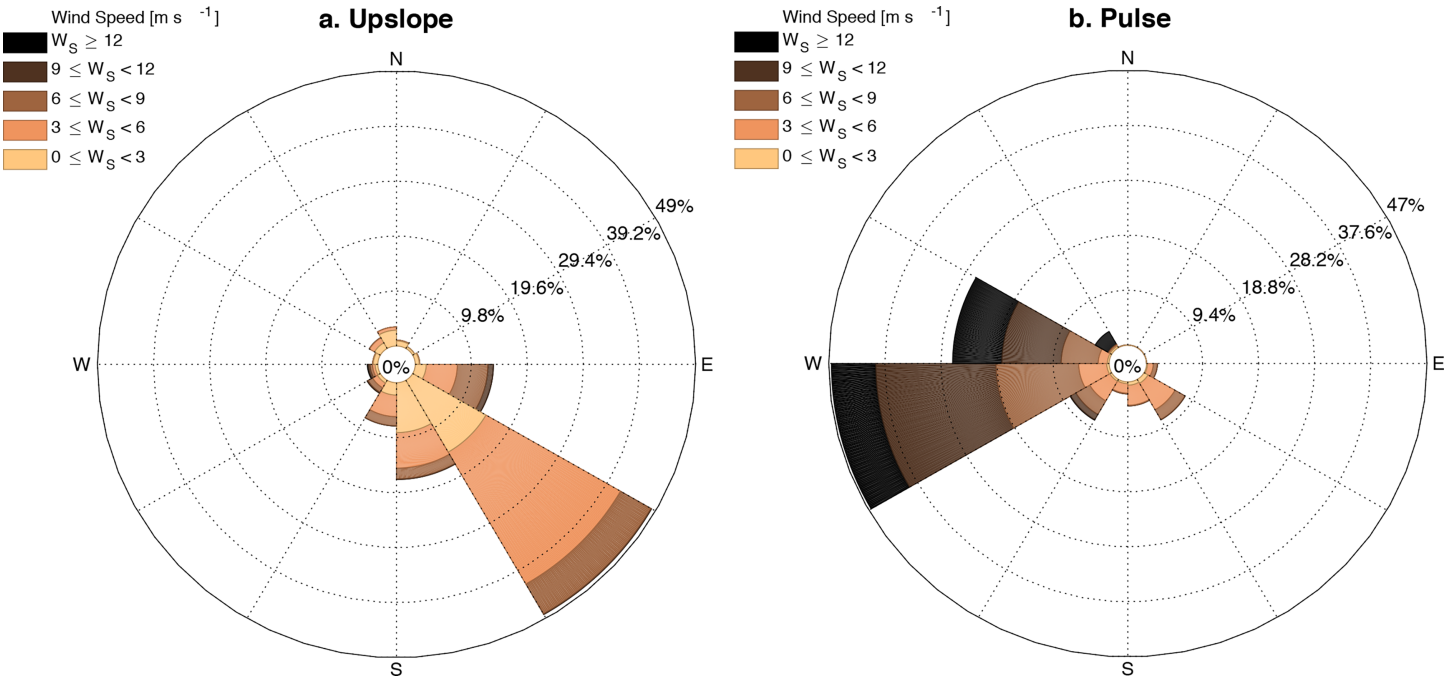

Fig. 6. Wind roses for the (a) upslope and (b) pulsed snowfall regimes observed during HiLaMS. Figure from S19.

as they flow up the eastern flank of the mountain range. The other snowfall regime exhibited bands of very heavy snowfall formed in the presence of strong westerly winds. Such winds indicate airflow coming over the mountains to the west of Haukeliseter and would be consistent with the presence of wave breaking on the lee side of the ridge. Accordingly, S19 labeled the easterly snow regime "upslope" and the westerly snow regime "pulsed," where wind roses for the regime events are shown in Fig. 6.

Retrieved snowfall values from the combined MRR–PIP–MASC retrieval scheme agreed well with MET-Norway DFAR observations for both snowfall regimes. For the low-wind, easterly upslope regimes, use of PIP PSD and fall speed observations with the RA particle model resulted in a difference of −0.4% for cumulative accumulation totals over the season at Haukeliseter. Typical discrepancies were ±35% for individual snow events. For the high-wind westerly pulsed regime, the scheme performed poorly when using surface, in situ observations due to the presence of heavy blowing snow. However, use of the *CloudSat* PSD–temperature parameterization, fall speed from MRR Doppler measurements, and the RA model generated a difference of +16% relative to the DFAR for snowfall accumulations for the season.

Although the optimal combination of measurements for the retrieval varied with snowfall regime, retrieval success depended to the first order upon the selection of a snowflake particle model well matched to scene meteorological conditions. For example, the use of the LRA particle model assumed in the *CloudSat* 2C-SNOW-PROFILE product resulted in seasonal accumulations of +139% relative to the DFAR for the pulsed regime, as compared to just +16% with use of the RA model. Opposite conclusions, however, were found for the snow events observed at Kiruna. Figure 7 suggests that use of the LRA better matches SMHI snow gauge observations for the colder and drier conditions observed near Kiruna than the RA model that worked well for Haukeliseter. These findings can be explained by D-ICI images that suggest more-pristine type snowflakes at the Kiruna site as shown in Fig. SB2. In general, HiLaMS retrieval results agreed well in spirit with recent studies that demonstrated the benefits of exploiting in situ microphysical observations to improve estimates of snowfall rate derived from radar reflectivities (Souverijns et al. 2017; von Lerber et al. 2017; Schoger et al. 2021).

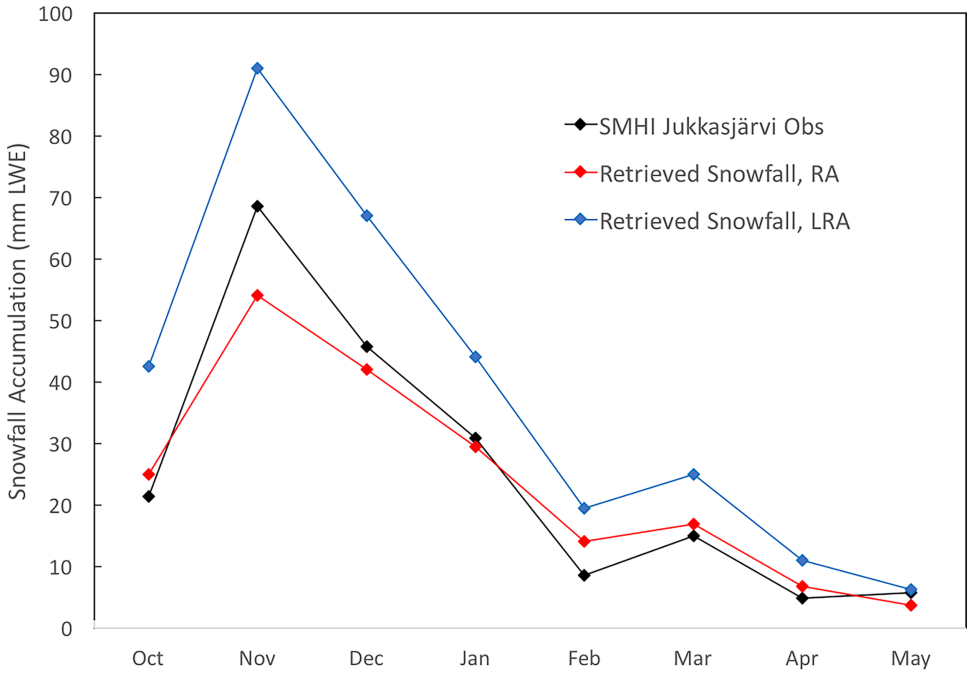

Fig. 7. Observed SMHI snowfall accumulations in liquid water equivalent (LWE) plotted vs retrieved values assuming the LRA and RA particle models. It is assumed the single-fence snow gauge at Jukkasjärvi undercatches snowfall as discussed in the "Haukeliseter snow gauge studies" sidebar.

Snowfall regimes at Haukeliseter and Kiruna. Building on the preliminary regime classification in S19, Shates et al. (2021) identified and characterized the dominant snowfall regimes observed at both Haukeliseter and Kiruna during HiLaMS. Events were classified based upon snow event macrophysical properties, macrophysical structure, and local weather conditions placed in context of coincident synoptic-scale environment and atmospheric thermodynamic profiles. Their analysis suggested that each shallow, deep, and intermittent snowfall regimes are observed at both locations. Figure 8 shows 2D histograms of MRR reflectivity versus height for these snowfall regimes at Haukeliseter and Kiruna.

Shates et al. (2021) discussed how these regimes varied both for a given site and across location. For example, shallow regimes produce light, long-lasting snowfall, and occur under regions of high pressure and large-scale subsidence. They are more common at Kiruna than at the mountainous Haukeliseter site. Conversely, deep snowfall regime produces moderate snowfall rates under relatively weak synoptic disturbances. The intermittent snowfall regime is associated with high impact snowfall and occurs during extremely warm and moist conditions associated with strong extratropical cyclogenesis. While qualitative similarities exist between regimes at both sites, there are notable differences between their characteristics at each site. For example, the intermittent regime at Haukeliseter produced more high reflectivity and deeper events than those at Kiruna, likely a result of intense storms off the warm Gulf Stream. Snowfall profiles for all three regimes in Haukeliseter were complicated by the impact of the mountainous terrain.

Shates et al. (2021) also determined the synoptic-scale conditions, thermodynamic structure, and microphysics associated with each of these snow regimes, providing constraints for assessing their representation in NWP or climate model simulations. Figure 9 shows mean sea level pressure and 500-hPa heights for snowfall regimes for both Haukeliseter and Kiruna. If model simulations are to faithfully represent snow regimes at each site, they should be able to replicate these patterns as well as the 2D histograms shown in Fig. 8. Simulations also should

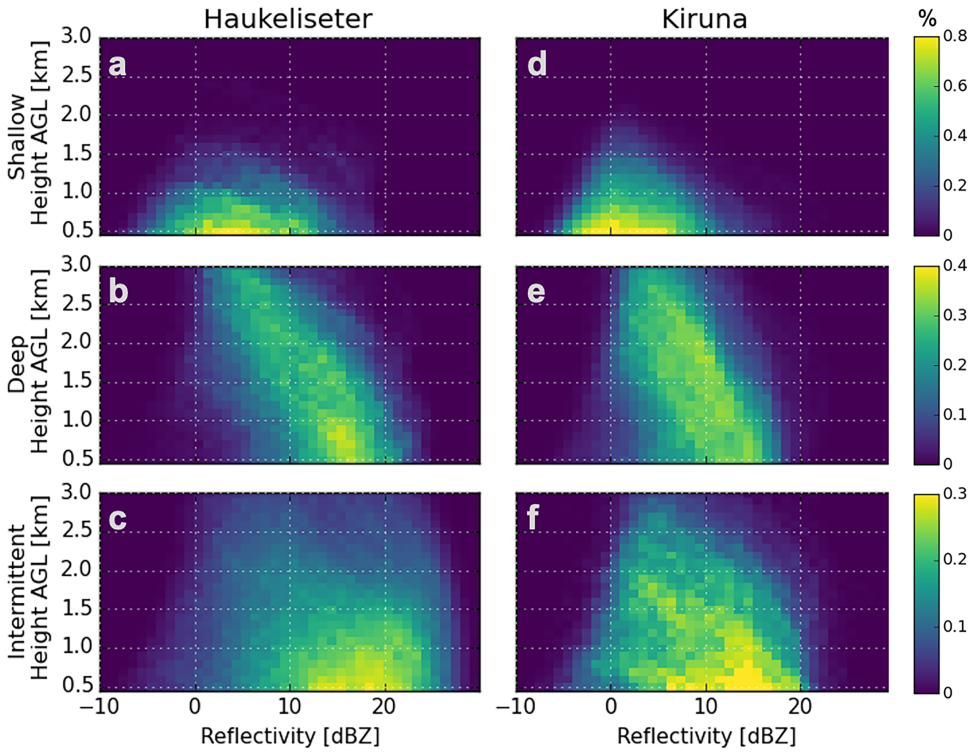

Fig. 8. Two-dimensional histograms of MRR reflectivity vs height above ground level for the snowfall regimes observed at (left) Haukeliseter and (right) Kiruna. Figure modified from Shates et al. (2021).

generate snowfall regimes with similar snowfall production and relative frequency for sites across the high latitudes as those observed from campaigns such as HiLaMS.

Evaluation of snowfall production in HARMONIE-AROME. Retrieved profiles of snow water generated from HiLaMS observations were used to evaluate the ability of HARMONIE-AROME, a mesoscale nonhydrostatic, convection-permitting NWP model, to forecast surface snowfall accumulations and vertical profiles of SWC for the Haukeliseter site. It uses the single-moment ICE3 bulk microphysics scheme to represent cloud microphysics which simulates mass mixing ratios of cloud water and ice, rain, snow, and graupel (Caniaux et al. 1994; Pinty and Jabouille 1998). It is used for operational short range forecasts in the Scandinavian countries through implementation in the Meteorological Cooperation on Operational Numeric Weather Prediction ensemble prediction system (MEPS) employed at MET-Norway and SMHI.

Snow production in NWP models exhibit well-known sensitivity to microphysical schemes. In HARMONIE-AROME, early versions produced too much cloud ice with its default ICE3 cloud microphysics scheme, prompting refinements to modify low-level and cirrus cloud ice representation (Müller et al. 2017). Engdahl et al. (2020a) showed that despite these improvements, the ICE3 microphysics scheme depleted supercooled liquid water too quickly and produced a surplus of snow and graupel. For this reason, Engdahl et al. (2020a) introduced a series of changes to the ICE3 scheme based on the parameterization that included ice nucleation, riming, and accretion parameterizations. Idealized 1D experiments showed that the modified scheme prolonged the existence and produced higher amounts of supercooled liquid water.

Hellmuth et al. (2021) compared HARMONIE-AROME simulated surface snowfall accumulations using both the base microphysical parameterization scheme with corrections (CTRL) as noted in Engdahl et al. (2020b) and the refined scheme with updated nucleation and riming (ICE-T) with MET-Norway DFAR observations for winter season 2016/17 at Haukeliseter. They found that the CTRL and ICE-T schemes overestimated seasonal surface snowfall accumulations by

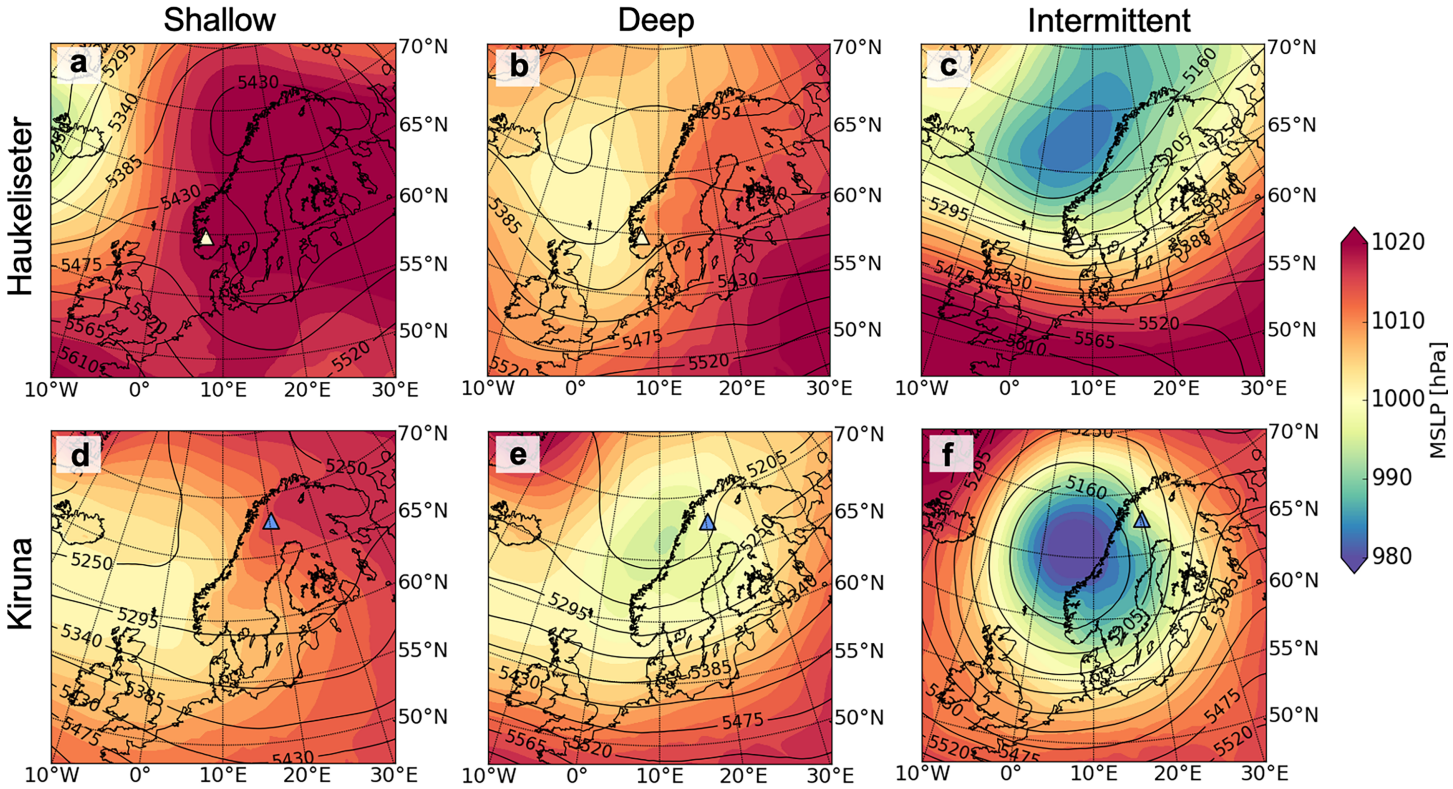

Fig. 9. Composites of the MSLP and 500-hPa heights for observed shallow, deep, and intermittent snowfall regimes for both Haukeliseter and Kiruna sites based upon ERA5 reanalysis. Figure modified from Shates et al. (2021).

+43.8% and +59.2%, respectively, relative to DFAR observations. Both schemes performed better relative to DFAR for the low-wind, easterly upslope regime (CTRL +1.8%, ICE-T +5.0%) than for the high-wind, westerly pulsed regime (CTRL +59.3%, ICE-T +79.2%); see Table 1.

However, Fig. 10 shows that, in contrast to surface forecasts where the model parameterizations over predicted snowfall amount, both CTRL and ICE-T simulations underestimate the SWC aloft relative to the MRR retrievals. This basic trend holds across snowfall regime and wind speed categories with minor exceptions for the Haukeliseter site. These results highlight the ability of HiLaMS instrumentation to identify potential biases in NWP simulations of the processes that link surface snow accumulation to snow water aloft. The consideration of surface accumulation or vertical SWC profile values alone would lead to misleading conclusions regarding model snowfall production.

A path forward for understanding snowfall impacts

HiLaMS activities demonstrated the usefulness of the core MRR–PIP–MASC instrumentation suite for snowfall process studies. Given the highly portable nature of the instrumentation package, the studies presented in this work could be replicated for other underrepresented

Table 1. HiLaMS snowfall accumulation values from DFAR observations, MRR-based retrieval algorithm (OESR), and HARMONIE-AROME CTRL and ICE-T parameterization scheme runs. Values are presented for easterly and westerly snowfall regimes and total snowfall (modified from Hellmuth et al. 2021).

	West (mm)	Diff (%)	East (mm)	Diff (%)	Total (mm)	Diff (%)
DFAR	146.5	–	54.0	–	200.5	–
OESR	157.2	+7.3	65.1	+20.5	222.3	+10.9
CTRL	233.3	+59.3	55.0	+1.8	288.3	+43.8
ICE-T	262.4	+79.2	56.7	+5.0	319.2	+59.2

locations and climates. These initial studies also lay the foundation for further analyses exploring the linkages between hydrological, dynamical, and radiative processes as related to snowfall.

HiLaMS enabled the development and evaluation of a new combined MRR and in situ microphysical property retrieval scheme to estimate surface snowfall accumulations. Our optimal-estimation retrieval scheme performs well at both Haukeliseter and Kiruna locations and demonstrates the synergy between the MRR reflectivities and MASC particle habits for addressing the fundamental need to select appropriate particle models (dimension–mass–scattering relationships) matched to environmental snow conditions. The particle model that worked well for Haukeliseter was a poor match for Kiruna, and vice versa, due to contrasting meteorological conditions at each site. These results articulate the need for augmenting the range of snow regimes for which such particle models are available to constrain global snowfall algorithms such as those used by the *CloudSat* mission. A logical next step would be to refine the *CloudSat* particle models using real-world observations of snowflake shape, PSD, and degree of riming available from HiLaMS instrumentation when placed in context of snow regime dynamic and thermodynamic environments. For example, Leinonen et al. (2021) developed a technique to estimate snowflake mass and geometry from MASC images. Ideally, these refined models would be compared with existing community particle models to determine which best fits the snowfall regimes at each site (e.g., see Petty and Huang 2010; Kulie et al. 2014; Leinonen and Szyrmer 2015).

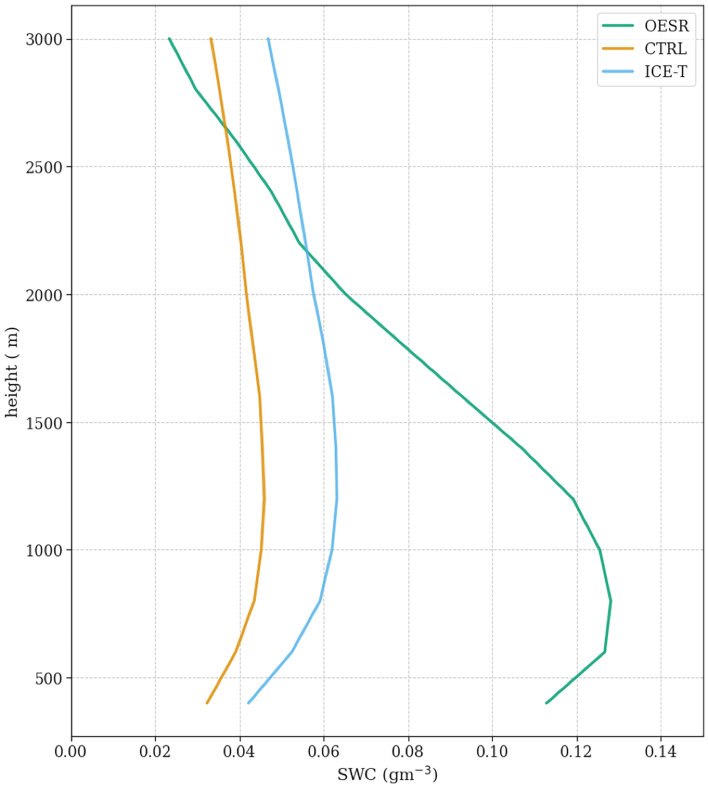

Fig. 10. Seasonal means of SWC plotted vs height for the retrieval (OESR) and CTRL and ICE-T parameterization schemes. Figure modified from Hellmuth et al. (2021).

HiLaMS analyses also illustrates how the MRR–PIP–MASC can be used to characterize the predominant snowfall regimes in challenging high-latitude locations. For example, Shates et al. (2021) documented three snowfall regimes with distinct macrophysical structures (shallow, deep, and intermittent) at each site but identified key differences in their frequency, microphysical properties, snowfall production, synoptic-scale dynamics, and thermodynamic structure. Hellmuth et al. (2021) demonstrated how such measurements can be used to evaluate snowfall forecasts in the HARMONIE-AROME model used for operational forecasts in Scandinavia. They found the model overestimated surface snowfall while simultaneously underestimating SWC values aloft. Both studies provide valuable constraints on the representation of snowfall in NWP and climate models.

Future deployments of HiLaMS instrumentation to novel sites would provide a more complete sampling of global dominant snowfall regimes and their meteorological environments. Lower-latitude deployments would complement similar, existing efforts at the Falling Snowfall Observatory in Japan (Ishizaka et al. 2013; Steenburgh and Nakai 2020) and the Marquette, Michigan, enhanced snow observation suite (Pettersen et al. 2020b; Kulie et al. 2021). Deeper

analysis of the spatial and temporal evolution of MRR reflectivities, Doppler velocity, and spectral width fields will offer insights into processes by identifying areas of riming, aggregation, evaporation, etc. within the storms (e.g., Matrosov et al. 2007). Such assessments of bulk processes are enhanced by verifying their consistency with snowflake microphysical properties such as PSD, habit, and degree of riming derived from the PIP and MASC on the ground (Garrett and Yutter 2014; Praz et al. 2017; Leinonen et al. 2021). Inclusion of portable multifrequency radar would provide additional information on both snowfall microphysical properties and processes (e.g., Moisseev et al. 2015; Leinonen et al. 2018; Mason et al. 2018; Ori et al. 2020; Planat et al. 2021).

Augmenting the core HiLaMS suite with sensors, such as upward and downward viewing broadband radiometers, offers the potential for addressing several broader climate and weather problems linking the hydrologic and energy cycles. Radiometer measurements would quantify the downwelling shortwave and longwave radiation for each of the identified snowfall regimes at each site. Downwelling radiation measurements would be particularly illuminating for understanding the impact of lightly precipitating, mixed-phase snowfall regimes, whose radiative characteristics are dominated by the amount of liquid water aloft, on surface energy balance. The partitioning between ice and water phases in these cloud systems is notoriously difficult to model in climate simulations (McCoy et al. 2016; Tan and Storelvmo 2019), resulting in potential model biases in both snowfall production and surface radiation budgets. Coincident measurements from lidar and/or passive microwave measurements available at partner sites could further constrain cloud phase in such studies. Likewise, coincident measurements of surface albedo may help to determine how the snowfall modifies the environment and feedbacks on snow regime evolution.

Overall, HiLaMS provided new insights into snowfall regimes, observational techniques, and NWP forecasting for two meteorologically distinct sites in Scandinavia. As such, we endorse the continued deployment of the highly portable MRR–PIP–MASC instrumentation. We note, however, that each of these instruments could be replaced with similar equipment, e.g., D-ICI substitution for the MASC at Kiruna. The core objective is to generate high-quality, coincident observations of key snowfall properties for unique locations and snowfall regimes. Such observations, applied in combination with complementary instrumentation and analysis techniques provided by the wider atmospheric community, should help unravel the complex relationships between snowfall processes and a changing climate.

Acknowledgments. We thank Walt Petersen and Larry Bliven of NASA for use of the PIP. We thank Lars Norin and Richard Moore for useful discussions outlining the project. U.S. efforts were supported through National Science Foundation Grants 1531930 and 1531690 and through NASA NIP Grant 80NSSC21K0931. FH was funded through European Research Council (ERC) Grant StG 758005. BJKE was funded by the Norwegian Research Council Grant 224106/E10.

Data availability statement. The dataset on which this paper is based is too large to be retained or publicly archived with available resources. Documentation and methods used to support this study are available from S. J. Cooper (steve.cooper@utah.edu).

References

Bekryaev, R. V., I. V. Polyakov, and V. A. Alexeev, 2010: Role of polar amplification in long-term surface air temperature variations and modern Arctic warming. *J. Climate*, **23**, 3888–3906, https://doi.org/10.1175/2010JCLI3297.1.

Bengtsson, L., and Coauthors, 2017: The HARMONIE–AROME model configuration in the ALADIN–HIRLAM NWP system. *Mon. Wea. Rev.*, **145**, 1919–1935, https://doi.org/10.1175/MWR-D-16-0417.1.

Bennartz, R., and Coauthors, 2013: July 2012 Greenland melt extent enhanced by low-level liquid clouds. *Nature*, **496**, 83–86, https://doi.org/10.1038/nature12002.

Berne, A., J. Grazioli, and C. Genthon, 2017: Snowfall rate estimates derived from a Micro Rain Radar (MRR) at the Dumont d'Urville station, Adelie Land, East Antarctica, link to netCDF file. PANGAEA, accessed 28 February 2022, https://doi.org/10.1594/PANGAEA.882565.

Betts, A. K., R. Desjardins, D. Worth, S. Wang, and J. Li, 2014: Coupling of winter climate transitions to snow and clouds over the prairies. *J. Geophys. Res. Atmos.*, **119**, 1118–1139, https://doi.org/10.1002/2013JD021168.

Bindoff, N. L., and Coauthors, 2013: Detection and attribution of climate change: From global to regional. *Climate Change 2013: The Physical Science Basis*, T. F. Stocker et al., Eds., Cambridge University Press, 867–962.

Brousseau, P., Y. Seity, D. Ricard, and J. Léger, 2016: Improvement of the forecast of convective activity from the AROME-France system. *Quart. J. Roy. Meteor. Soc.*, **142**, 2231–2243, https://doi.org/10.1002/qj.2822.

Brown, R., 2000: Northern Hemisphere snow cover variability and change, 1915–97. *J. Climate*, **13**, 2339–2355, https://doi.org/10.1175/1520-0442(2000)013<2339:NHSCVA>2.0.CO;2.

Caniaux, G., J.-L. Redelsperger, and J.-P. Lafore, 1994: A numerical study of the stratiform region of a fast-moving squall line. Part I: General description and water and heat budgets. *J. Atmos. Sci.*, **51**, 2046–2074, https://doi.org/10.1175/1520-0469(1994)051<2046:ANSOTS>2.0.CO;2.

Chapman, W. L., and J. E. Walsh, 1993: Recent variations of sea ice and air temperature in high latitudes. *Bull. Amer. Meteor. Soc.*, **74**, 33–47, https://doi.org/10.1175/1520-0477(1993)074<0033:RVOSIA>2.0.CO;2.

Cohen, J., and D. Rind, 1991: The effect of snow cover on the climate. *J. Climate*, **4**, 689–706, https://doi.org/10.1175/1520-0442(1991)004<0689:TEOSCO>2.0.CO;2.

——, J. Furtado, M. Barlow, V. Alexeev, and J. Cherry, 2012: Arctic warming, increasing fall snow cover and widespread boreal winter cooling. *Environ. Res. Lett.*, **7**, 014007, https://doi.org/10.1088/1748-9326/7/1/014007.

Cooper, S. J., N. B. Wood, and T. S. L'Ecuyer, 2017: A variational technique to estimate snowfall rate from coincident radar, snowflake, and fallspeed observations. *Atmos. Meas. Tech.*, **10**, 2557–2571, https://doi.org/10.5194/amt-10-2557-2017.

Crook, J. A., P. M. Forster, and N. Stuber, 2011: Spatial patterns of modeled climate feedback and contributions to temperature response and polar amplification. *J. Climate*, **24**, 3575–3592, https://doi.org/10.1175/2011JCLI3863.1.

Curry, J. A., D. Randall, W. B. Rossow, and J. L. Schramm, 1996: Overview of Arctic cloud and radiation characteristics. *J. Climate*, **9**, 1731–1764, https://doi.org/10.1175/1520-0442(1996)009<1731:OOACAR>2.0.CO;2.

Draine, B. T., and P. J. Flatau, 1994: Discrete-dipole approximation for scattering calculations. *J. Opt. Soc. Amer.*, **11A**, 1491–1499, https://doi.org/10.1364/JOSAA.11.001491.

Engdahl, B. J. K., G. Thompson, and L. Bengtsson, 2020a: Improving the representation of supercooled liquid water in the HARMONIE-AROME weather forecast model. *Tellus*, **72A**, 1697603, https://doi.org/10.1080/16000870.2019.1697603.

——, B. E. K. Nygaard, V. W. Losnedal, G. Thompson, and L. Bengtsson, 2020b: Effects of the ICE-T microphysics scheme in HARMONIE-AROME on estimated ice loads on transmission lines. *Cold Reg. Sci. Technol.*, **179**, 103139, https://doi.org/10.1016/j.coldregions.2020.103139.

Gardner, A. S., and Coauthors, 2013: A reconciled estimate of glacier contributions to sea level rise: 2003 to 2009. *Science*, **340**, 852–857, https://doi.org/10.1126/science.1234532.

Garrett, T. J., and S. E. Yutter, 2014: Observed influence of riming, temperature, and turbulence on the fallspeed of solid precipitation. *Geophys. Res. Lett.*, **41**, 6515–6522, https://doi.org/10.1002/2014GL061016.

——, C. Fallgatter, K. Shurko, and D. Howlett, 2012: Fall speed measurement and high-resolution multi-angle photography of hydrometeors in free fall. *Atmos. Meas. Tech.*, **5**, 2625–2633, https://doi.org/10.5194/amt-5-2625-2012.

Geerts, B., 2019: Cold-Air Outbreaks in the Marine Boundary Layer Experiment (COMBLE) science implementation plan. U.S. Dept. of Energy Office of Science Rep. DOE/SC-ARM-19-002, 38 pp., www.osti.gov/servlets/purl/1499128.

Gisnås, K., and Coauthors, 2017: Permafrost map for Norway, Sweden and Finland. *Permafrost Periglacial Processes*, **28**, 359–378, https://doi.org/10.1002/ppp.1922.

Goodison, B. E., P. Y. T. Louie, and D. Yang, 1998: WMO solid precipitation measurement intercomparison. WMO Instruments and Observing Methods Rep. 67, 212 pp., https://library.wmo.int/doc_num.php?explnum_id=9694.

Grazioli, J., C. Genthon, B. Boudevillain, C. Duran-Alarcon, M. Del Guasta, J.-B. Madeleine, and A. Berne, 2017: Measurements of precipitation in Dumont d'Urville, Adélie Land, East Antarctica. *Cryosphere*, **11**, 1797–1811, https://doi.org/10.5194/tc-11-1797-2017.

Hellmuth, F., B. J. K. Engdahl, T. Storelvmo, R. O. David, and S. J. Cooper, 2021: Snowfall model validation using surface observations and an optimal estimation snowfall retrieval. *Wea. Forecasting*, **36**, 1827–1842, https://doi.org/10.1175/WAF-D-20-0220.1.

Holland, M. M., and C. M. Bitz, 2003: Polar amplification of climate change in coupled models. *Climate Dyn.*, **21**, 221–232, https://doi.org/10.1007/s00382-003-0332-6.

——, ——, and L.-B. Tremblay, 2006: Future abrupt reductions in the summer Arctic sea ice. *Geophys. Res. Lett.*, **33**, L23503, https://doi.org/10.1029/2006GL028024.

Hudak, D., H. Barker, P. Rodriguez, and D. Donovan, 2006: The Canadian CloudSat validation project. *Fourth European Conf. on Radar in Hydrology and Meteorology*, Barcelona, Spain, CRAHI UPC, P11.6, www.crahi.upc.edu/ERAD2006/proceedingsMask/00165.pdf.

Intrieri, J. M., C. W. Fairall, M. D. Shupe, P. O. G. Persson, E. L. Andreas, P. S. Guest, and R. E. Moritz, 2002: An annual cycle of Arctic surface cloud forcing at SHEBA. *J. Geophys. Res.*, **107**, 8039, https://doi.org/10.1029/2000JC000439.

Ishizaka, M., H. Motoyoshi, S. Nakai, T. Shiina, T. Kumakura, and K. Muramoto, 2013: A new method for identifying the main type of solid hydrometeors contributing to snowfall from measured size-fall speed relationship. *J. Meteor. Soc. Japan*, **91**, 747–762, https://doi.org/10.2151/jmsj.2013-602.

Jacob, T., J. Wahr, W. T. Pfeffer, and S. Swenson, 2012: Recent contributions of glaciers and ice caps to sea level rise. *Nature*, **482**, 514–518, https://doi.org/10.1038/nature10847.

Joos, H., and H. Wernli, 2012: Influence of microphysical processes on the potential vorticity development in a warm conveyor belt: A case-study with the limited-area model COSMO. *Quart. J. Roy. Meteor. Soc.*, **138**, 407–418, https://doi.org/10.1002/qj.934.

Klugmann, D., K. Heinsohn, and H. Kirtzel, 1996: A low cost 24 GHz FM-CW Doppler radar rain profiler. *Contrib. Atmos. Phys.*, **69**, 247–253.

Kochendorfer, J., and Coauthors, 2017: Analysis of single-Alter-shielded and unshielded measurements of mixed and solid precipitation from WMO-SPICE. *Hydrol. Earth Syst. Sci.*, **21**, 3525–3542, https://doi.org/10.5194/hess-21-3525-2017.

——, and Coauthors, 2018: Testing and development of transfer functions for weighing precipitation gauges in WMO-SPICE. *Hydrol. Earth Syst. Sci.*, **22**, 1437–1452, https://doi.org/10.5194/hess-22-1437-2018.

——, and Coauthors, 2021: How well are we measuring snow post-SPICE? *Bull. Amer. Meteor. Soc.*, **103**, E370–E388, https://doi.org/10.1175/BAMS-D-20-0228.1.

Kollias, P., B. P. Treserras, and A. Protat, 2019: Calibration of the 2007–2017 record of Atmospheric Radiation Measurements cloud radar observations using

CloudSat. *Atmos. Meas. Tech.*, **12**, 4949–4964, https://doi.org/10.5194/amt-12-4949-2019.

Kuhn, T., and S. Vázquez-Martín, 2020: Microphysical properties and fall speed measurements of snow ice crystals using the Dual Ice Crystal Imager (D-ICI). *Atmos. Meas. Tech.*, **13**, 1273–1285, https://doi.org/10.5194/amt-13-1273-2020.

Kulie, M. S., and R. Bennartz, 2009: Utilizing spaceborne radars to retrieve dry snowfall. *J. Appl. Meteor. Climatol.*, **48**, 2564–2580, https://doi.org/10.1175/2009JAMC2193.1.

——, M. J. Hiley, R. Bennartz, S. Kneifel, and S. Tanelli, 2014: Triple-frequency radar reflectivity signatures of snow: Observations and comparisons with theoretical ice particle scattering models. *J. Appl. Meteor. Climatol.*, **53**, 1080–1098, https://doi.org/10.1175/JAMC-D-13-066.1.

——, and Coauthors, 2021: Snowfall in the northern Great Lakes: Lessons learned from a multisensor observatory. *Bull. Amer. Meteor. Soc.*, **102**, E1317–E1339, https://doi.org/10.1175/BAMS-D-19-0128.1.

Leinonen, J., and W. Szyrmer, 2015: Radar signatures of snowflake riming: A modeling study. *Earth Space Sci.*, **2**, 346–358, https://doi.org/10.1002/2015EA000102.

——, and Coauthors, 2018: Retrieval of snowflake microphysical properties from multifrequency radar observations. *Atmos. Meas. Tech.*, **11**, 5471–5488, https://doi.org/10.5194/amt-11-5471-2018.

——, J. Grazioli, and A. Berne, 2021: Reconstruction of the mass and geometry of snowfall particles from Multi-Angle Snowflake Camera (MASC) images. *Atmos. Meas. Tech.*, **14**, 6851–6866, https://doi.org/10.5194/amt-14-6851-2021.

Lenaerts, J., E. Meijgaard, M. R. Broeke, S. R. M. Ligtenberg, M. Horwath, and E. Isaksson, 2013: Recent snowfall anomalies in Dronning Maud Land, East Antarctica, in a historical and future climate perspective. *Geophys. Res. Lett.*, **40**, 2684–2688, https://doi.org/10.1002/grl.50559.

Maahn, M., and P. Kollias, 2012: Improved micro rain radar snow measurements using Doppler spectra post-processing. *Atmos. Meas. Tech.*, **5**, 2661–2673, https://doi.org/10.5194/amt-5-2661-2012.

Manabe, S., and R. J. Stouffer, 1980: Sensitivity of a global climate model to an increase of CO_2 concentration in the atmosphere. *J. Geophys. Res.*, **85**, 5529–5554, https://doi.org/10.1029/JC085iC10p05529.

Mason, S. L., C. J. Chiu, R. J. Hogan, D. Moisseev, and S. Kneifel, 2018: Retrievals of riming and snow density from vertically pointing Doppler radars. *J. Geophys. Res. Atmos.*, **123**, 13 807–13 834, https://doi.org/10.1029/2018JD028603.

Matrosov, S. Y., K. A. Clark, and D. E. Kingsmill, 2007: A polarimetric radar approach to identify rain, melting-layer, and snow regions for applying corrections to vertical profiles of reflectivity. *J. Appl. Meteor. Climatol.*, **46**, 154–166, https://doi.org/10.1175/JAM2508.1.

McCoy, D. T., I. Tan, D. L. Hartmann, M. D. Zelinka, and T. Storelvmo, 2016: On the relationships among cloud cover, mixed-phase partitioning, and planetary albedo in GCMs. *J. Adv. Model. Earth Syst.*, **8**, 650–668, https://doi.org/10.1002/2015MS000589.

McIlhattan, E. A., T. S. L'Ecuyer, and N. B. Miller, 2017: Observational evidence linking Arctic supercooled liquid cloud biases in CESM to snowfall processes. *J. Climate*, **30**, 4477–4495, https://doi.org/10.1175/JCLI-D-16-0666.1.

Moisseev, D. N., S. Lautaportti, J. Tyynela, and S. Lim, 2015: Dual polarization radar signatures in snowstorms: Role of snowflake aggregation. *J. Geophys. Res. Atmos.*, **120**, 12 644–12 655, https://doi.org/10.1002/2015JD023884.

Morrison, H., G. de Boer, G. Feingold, J. Harrington, M. D. Shupe, and K. Sulia, 2012: Resilience of persistent Arctic mixed-phase clouds. *Nat. Geosci.*, **5**, 11–17, https://doi.org/10.1038/ngeo1332.

Müller, M., and Coauthors, 2017: AROME-MetCoOp: A Nordic convective-scale operational weather prediction model. *Wea. Forecasting*, **32**, 609–627, https://doi.org/10.1175/WAF-D-16-0099.1.

Myagkov, A., S. Kneifel, and T. Rose, 2020: Evaluation of the reflectivity calibration of W-band radars based on observations in rain. *Atmos. Meas. Tech.*, **13**, 5799–5825, https://doi.org/10.5194/amt-13-5799-2020.

Nicholls, N., G. V. Gruza, J. Jouzel, T. R. Karl, L. A. Ogallo, and D. E. Parker, 1996: Observed climate variability and change. *Climate Change 1995: The Science of Climate Change*, J. T. Houghton et al., Eds., Cambridge University Press, 133–192.

Nitu, R., and Coauthors, 2018: WMO Solid Precipitation Intercomparison Experiment (SPICE) (2012–2015). WMO Instruments and Observing Methods Rep. 131, 1445 pp.

Ori, D., V. Schemann, M. Karrer, J. Neto, L. Terzi, A. Seifert, and S. Kneifel, 2020: Evaluation of ice particle growth in ICON using statistics of multi-frequency Doppler cloud radar observations. *Quart. J. Roy. Meteor. Soc.*, **146**, 3830–3849, https://doi.org/10.1002/qj.3875.

Palerme, C., J. E. Kay, C. Genthon, T. L'Ecuyer, N. B. Wood, and C. Claud, 2014: How much snow falls on the Antarctic ice sheet? *Cryosphere*, **8**, 1577–1587, https://doi.org/10.5194/tc-8-1577-2014.

——, C. Genthon, C. Claud, J. E. Kay, N. B. Wood, and T. L'Ecuyer, 2017: Evaluation of current and projected Antarctic precipitation in CMIP5 models. *Climate Dyn.*, **48**, 225–239, https://doi.org/10.1007/s00382-016-3071-1.

Petäjä, T., and Coauthors, 2016: BAECC: A field campaign to elucidate the impact of biogenic aerosols on clouds and climate. *Bull. Amer. Meteor. Soc.*, **97**, 1909–1928, https://doi.org/10.1175/BAMS-D-14-00199.1.

Pettersen, C., R. Bennartz, A. J. Merrelli, M. D. Shupe, D. D. Turner, and V. P. Walden, 2018: Precipitation regimes over central Greenland inferred from 5 years of ICECAPS observations. *Atmos. Chem. Phys.*, **18**, 4715–4735, https://doi.org/10.5194/acp-18-4715-2018.

——, and Coauthors, 2020a: The Precipitation Imaging Package: Assessment of microphysical and bulk characteristics of snow. *Atmosphere*, **11**, 785, https://doi.org/10.3390/atmos11080785.

——, M. S. Kulie, L. F. Bliven, A. J. Merrelli, W. A. Petersen, T. J. Wagner, D. B. Wolff, and N. B. Wood, 2020b: A composite analysis of snowfall modes from four winter seasons in Marquette, Michigan. *J. Appl. Meteor. Climatol.*, **59**, 103–124, https://doi.org/10.1175/JAMC-D-19-0099.1.

——, and Coauthors, 2021: The Precipitation Imaging Package: Phase partitioning capabilities. *Remote Sens.*, **13**, 2183, https://doi.org/10.3390/rs13112183.

Petty, G. W., and W. Huang, 2010: Microwave backscatter and extinction by soft ice spheres and complex snow aggregates. *J. Atmos. Sci.*, **67**, 769–787, https://doi.org/10.1175/2009JAS3146.1.

Pinty, J.-P., and P. Jabouille, 1998: A mixed-phased cloud parameterization for use in a mesoscale non-hydrostatic model: Simulations of a squall line and of orographic precipitation. *Proc. Conf. on Cloud Physics,* Everett, WA, Amer. Meteor. Soc., 17–21.

Planat, N., J. Gehring, E. Vignon, and A. Berne, 2021: Identification of snowfall microphysical processes from Eulerian vertical gradients of polarimetric radar variables. *Atmos. Meas. Tech.*, **14**, 4543–4564, https://doi.org/10.5194/amt-14-4543-2021.

Praz, C., Y.-A. Roulet, and A. Berne, 2017: Solid hydrometeor classification and riming degree estimation from pictures collected with a Multi-Angle Snowflake Camera. *Atmos. Meas. Tech.*, **10**, 1335–1357, https://doi.org/10.5194/amt-10-1335-2017.

Rasmussen, R., and Coauthors, 2012: How well are we measuring snow? The NOAA/FAA/NCAR winter precipitation test bed. *Bull. Amer. Meteor. Soc.*, **93**, 811–829, https://doi.org/10.1175/BAMS-D-11-00052.1.

Rodgers, C., 2000: *Inverse Methods for Atmospheric Sounding.* World Scientific, 240 pp.

Schäfler, A., and Coauthors, 2018: The North Atlantic Waveguide and Downstream Impact Experiment. *Bull. Amer. Meteor. Soc.*, **99**, 1607–1637, https://doi.org/10.1175/BAMS-D-17-0003.1.

Schirle, C. E., S. J. Cooper, M. A. Wolff, C. Pettersen, N. B. Wood, T. S. L'Ecuyer, T. Ilmo, and K. Nygård, 2019: Estimation of snowfall properties at a mountainous site in Norway using combined radar and in situ microphysical observations. *J. Appl. Meteor. Climatol.*, **58**, 1337–1352, https://doi.org/10.1175/JAMC-D-18-0281.1.

Schoger, S. Y., D. Moisseev, A. von Lerber, S. Crewell, and K. Ebell, 2021: Snowfall-rate retrieval for K- and W-band radar measurements designed in Hyytiälä, Finland, and tested at Ny-Ålesund, Svalbard, Norway. *J. Appl. Meteor. Climatol.*, **60**, 273–289, https://doi.org/10.1175/JAMC-D-20-0095.1.

Screen, J. A., and I. Simmonds, 2010: The central role of diminishing sea ice in recent Arctic temperature amplification. *Nature*, **464**, 1334–1337, https://doi.org/10.1038/nature09051.

Seity, Y., and Coauthors, 2011: The AROME-France convective-scale operational model. *Mon. Wea. Rev.*, **139**, 976–991, https://doi.org/10.1175/2010MWR3425.1.

Serreze, M. C., and J. A. Francis, 2006: The Arctic on the fast track of change. *Weather*, **61**, 65–69, https://doi.org/10.1256/wea.197.05.

——, and R. G. Barry, 2011: Processes and impacts of Arctic amplification: A research synthesis. *Global Planet. Change*, **77**, 85–96, https://doi.org/10.1016/j.gloplacha.2011.03.004.

Shates, J. A., C. Pettersen, T. S. L'Ecuyer, S. J. Cooper, M. S. Kulie, and N. B. Wood, 2021: High-latitude precipitation: Snowfall regimes at two distinct sites in Scandinavia. *J. Appl. Meteor. Climatol.*, **60**, 1127–1148, https://doi.org/10.1175/JAMC-D-20-0248.1.

Shepherd, A., and D. Wingham, 2007: Recent sea-level contributions of the Antarctic and Greenland ice sheets. *Science*, **315**, 1529–1532, https://doi.org/10.1126/science.1136776.

Shupe, M. D., and J. M. Intrieri, 2004: Cloud radiative forcing of the Arctic surface: The influence of cloud properties, surface albedo, and solar zenith angle. *J. Climate*, **17**, 616–628, https://doi.org/10.1175/1520-0442(2004)017<0616:CRFOTA>2.0.CO;2.

——, and Coauthors, 2013: High and dry: New observations of tropospheric and cloud properties above the Greenland ice sheet. *Bull. Amer. Meteor. Soc.*, **94**, 169–186, https://doi.org/10.1175/BAMS-D-11-00249.1.

——, and Coauthors, 2022: Overview of the MOSAiC expedition—Atmosphere. *Elementa*, **10**, 00060, https://doi.org/10.1525/elementa.2021.00060.

Smith, C. D., A. Ross, J. Kochendorfer, M. E. Earle, M. Wolff, S. Buisán, Y.-A. Roulet, and T. Laine, 2020: Evaluation of the WMO Solid Precipitation Intercomparison Experiment (SPICE) transfer functions for adjusting the wind bias in solid precipitation measurements. *Hydrol. Earth Syst. Sci.*, **24**, 4025–4043, https://doi.org/10.5194/hess-24-4025-2020.

Smith, W. M., and Coauthors, 2017: Arctic Radiation-IceBridge Sea and Ice Experiment (ARISE): The Arctic radiant energy system during the critical seasonal ice transition. *Bull. Amer. Meteor. Soc.*, **98**, 1399–1426, https://doi.org/10.1175/BAMS-D-14-00277.1.

Souverijns, N., A. Gossart, S. Lhermitte, I. V. Gorodetskaya, S. Kneifel, M. Maahn, F. L. Bliven, and N. P. M. van Lipzig, 2017: Estimating radar reflectivity—Snowfall rate relationships and their uncertainties over Antarctica by combining disdrometer and radar observations. *Atmos. Res.*, **196**, 211–223, https://doi.org/10.1016/j.atmosres.2017.06.001.

Steenburgh, W., and S. Nakai, 2020: Perspectives on sea- and lake-effect precipitation from Japan's "gosetsu chitai." *Bull. Amer. Meteor. Soc.*, **101**, E58–E72, https://doi.org/10.1175/BAMS-D-18-0335.1.

Stohl, A., C. Forster, and H. Sodemann, 2008: Remote sources of water vapor forming precipitation on the Norwegian west coast at 60°N—A tale of hurricanes and an atmospheric river. *J. Geophys. Res.*, **113**, D05102, https://doi.org/10.1029/2007JD009006.

Tan, I., and T. Storelvmo, 2019: Evidence of strong contributions from mixed-phase clouds to Arctic climate change. *Geophys. Res. Lett.*, **46**, 2894–2902, https://doi.org/10.1029/2018GL081871.

Tjernström, M., and Coauthors, 2014: The Arctic Summer Cloud Ocean Study (ASCOS): Overview and experimental design. *Atmos. Chem. Phys.*, **14**, 2823–2869, https://doi.org/10.5194/acp-14-2823-2014.

Van Tricht, K., and Coauthors, 2016: Clouds enhance Greenland ice sheet meltwater runoff. *Nat. Commun.*, **7**, 10266, https://doi.org/10.1038/ncomms10266.

Vavrus, S., 2007: The role of terrestrial snow cover in the climate system. *Climate Dyn.*, **29**, 73–88, https://doi.org/10.1007/s00382-007-0226-0.

Vázquez-Martín, S., T. Kuhn, and S. Eliasson, 2020: Shape dependence of falling snow crystals' microphysical properties using an updated shape classification. *Appl. Sci.*, **10**, 1163, https://doi.org/10.3390/app10031163.

——, ——, and ——, 2021a: Shape dependence of snow crystal fall speed. *Atmos. Chem. Phys.*, **21**, 7545–7565, https://doi.org/10.5194/acp-21-7545-2021.

——, ——, and ——, 2021b: Mass of different snow crystal shapes derived from fall speed measurements. *Atmos. Chem. Phys.*, **21**, 18669–18688, https://doi.org/10.5194/acp-21-18669-2021.

Verlinde, J., and Coauthors, 2007: The Mixed-Phase Arctic Cloud Experiment. *Bull. Amer. Meteor. Soc.*, **88**, 205–222, https://doi.org/10.1175/BAMS-88-2-205.

von Lerber, A., D. Moisseev, L. F. Bliven, W. Petersen, A.-M. Harri, and V. Chandrasekar, 2017: Microphysical properties of snow and their link to Z_e–S relations during BAECC 2014. *J. Appl. Meteor. Climatol.*, **56**, 1561–1582, https://doi.org/10.1175/JAMC-D-16-0379.1.

Wendisch, M., and Coauthors, 2019: The Arctic cloud puzzle: Using ACLOUD/PASCAL multiplatform observations to unravel the role of clouds and aerosol particles in Arctic amplification. *Bull. Amer. Meteor. Soc.*, **100**, 841–871, https://doi.org/10.1175/BAMS-D-18-0072.1.

Wolff, M. A., K. Isaksen, R. Braekkan, E. Alfnes, A. Petersen-Øverleir, and E. Ruud, 2013: Measurements of wind-induced loss of solid precipitation: Description of a Norwegian field study. *Hydrol. Res.*, **44**, 35–43, https://doi.org/10.2166/nh.2012.166.

——, ——, A. Petersen-Øverleir, K. Ødemark, T. Reitan, and R. Braekkan, 2015: Derivation of a new continuous adjustment function for correcting wind-induced loss of solid precipitation: Results of a Norwegian field study. *Hydrol. Earth Syst. Sci.*, **19**, 951–967, https://doi.org/10.5194/hess-19-951-2015.

Wood, N. B., and T. S. L'Ecuyer, 2018: Level 2C snow profile product process description and interface control document: Product version P1_R05. NASA JPL CloudSat Project Doc., revision 0, 26 pp., www.cloudsat.cira.colostate.edu/cloudsat-static/info/dl/2c-snow-profile/2C-SNOW-PROFILE_PDICD.P1_R05.rev0_.pdf.

——, and ——, 2021: What millimeter-wavelength radar reflectivity reveals about snowfall: An information-centric analysis. *Atmos. Meas. Tech.*, **14**, 869–888, https://doi.org/10.5194/amt-14-869-2021.

——, ——, A. J. Heymsfield, and G. L. Stephens, 2015: Microphysical constraints on millimeter-wavelength scattering properties of snow particles. *J. Appl. Meteor. Climatol.*, **54**, 909–931, https://doi.org/10.1175/JAMC-D-14-0137.1.